Metal-Pyridoxal Cooperativity in Nonenzymatic Transamination

Quentin Dherbassy, Robert J. Mayer, Kamila B. Muchowska, Joseph Moran

Metal-Pyridoxal Cooperativity in Nonenzymatic Transamination

Quentin Dherbassy*, Robert J. Mayer, Kamila B. Muchowska, Joseph Moran*

Université de Strasbourg, CNRS, ISIS & icFRC, 8 Allée Gaspard Monge, 67000 Strasbourg, France

Coenzymes, pyridoxal, catalysis, cofactor, mechanistic study, transamination

ABSTRACT: Coenzymes are involved in ≥30% of enzymatic reactions and likely predate enzymes, going back to prebiotic chemistry. However, they are considered poor organocatalysts, and thus their pre-enzymatic function remains unclear. Since metal ions are known to catalyze metabolic reactions in the absence of enzymes, here we explore the influence of metal ions on coenzyme catalysis under conditions relevant to the origin of life (20-75 °C, pH 5-7.5). Specifically, Fe or Al, the two most abundant metals in the Earth's crust, were found to exhibit substantial cooperative effects in transamination reactions catalyzed by pyridoxal (PL), a coenzyme scaffold used by roughly 4% of all enzymes. At 75 ºC and 7.5 mol% loading of PL/metal ion, Fe^{3+}-PL was found to be 90-fold faster at catalyzing transamination than PL alone and 174-fold faster than Fe^{3+} alone, whereas Al^{3+}-PL was 85-fold faster than PL alone and 38-fold faster than Al^{3+} alone. Under milder conditions, reactions catalyzed by Al^{3+}-PL were >1000 times faster than those catalyzed by PL alone. Pyridoxal phosphate (PLP) exhibited similar behavior to PL. Experimental and theoretical mechanistic studies indicate that the rate-determining step in the PL-metal-catalyzed transamination is different from metal-free and biological PL-based catalysis. Metal coordination to PL lowers the pK_a of the PL-metal complex by several units and slows the hydrolysis of imine intermediates by up to 259-fold. Coenzymes, specifically pyridoxal derivatives, could have exhibited useful catalytic function even before enzymes.

Introduction

Catalysis is central to life's processes and must have played a role dating back to its roots in prebiotic chemistry.[1–4] Amongst the various entities implicated in biological catalysis, cofactors such as metals,[5] metal ions,[6] and small organic molecules (coenzymes)[7,8] are the simplest and are, therefore, among the most likely to have appeared early in chemical evolution.[9] Cofactors are involved in over 60% of known enzymatic mechanisms,[10] and coenzymes are employed by over 30% of enzymes.[11] Metals and metal ions have been found to promote a wide variety of metabolic reactions in the absence of enzymes, a finding that sheds light on the potential prebiotic origins of metabolism.[12] Coenzymes, working independently or with metal ions, could also have played an important role in prebiotic chemistry.[13–15] However, only a few experimental investigations on the nonenzymatic catalytic properties of coenzymes have been carried out in such a context.[16] Coenzymes based on the pyridoxal scaffold, such as pyridoxal phosphate (PLP) and pyridoxamine (PMP), along with their vitaminic precursor pyridoxal (PL), represent a relevant case study for the potential role of coenzymes in prebiotic chemistry. They are widely used (~4% of known enzymes[17]) in a variety of biological reactions,[18] including in the transamination of amino acids and keto acids,[19] which is a central process in the biosynthesis of nearly all amino acids. PLP is essential in the co-catalysis of biological transamination because it couples two reversible half-reactions. In the first half-reaction, PLP accepts an amino

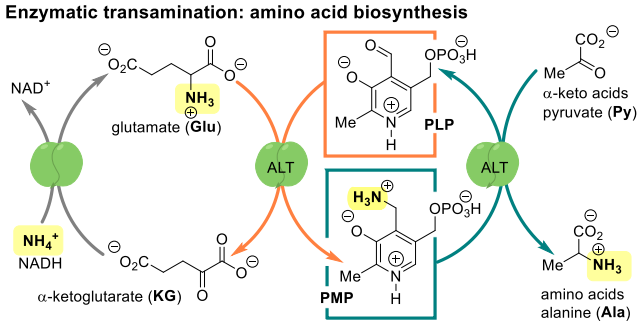

Scheme 1. Key steps of the enzymatic transamination of Glu to Ala, catalyzed by alanine aminotransferase (ALT) and the coenzymes pyridoxal-5'-phosphate (PLP) and pyridoxamine-5' phosphate (PMP).

group from an amino acid to form the corresponding keto acid and PMP under catalysis from an aminotransferase enzyme. In the second half-reaction, PMP transfers an amino group to an incoming keto acid to form the new amino acid and reform PLP, again with the help of aminotransferase (Scheme 1). Little is known about the catalytic potential of the pyridoxal scaffold for transamination in prebiotic chemistry before enzymes (Figure 1). The nonenzymatic transamination of amino and keto acids can hardly be avoided since it occurs spontaneously with some substrates[20] and is readily catalyzed by some metal ions[21] through a mechanism that we have recently studied in detail.[22] We wondered whether cooperation between metal ions and PL or PLP may have accelerated or enabled new prebiotic transamination reactions. In support of this idea, mechanistic

studies have demonstrated that half-reactions involving the pyridoxal scaffold can occur in the absence of enzymes[23–34] and are, in some cases, accelerated by metal ions.[24,35,31] However, inhibition by some metals has also been observed,[36] and thus merging these two independent half-reactions (cf. Scheme 1) into a productive process using catalytic quantities of PL or PLP, such that it might have relevance for prebiotic chemistry has so far proven elusive. Here we surveyed 18 of the most Earth-abundant metal ions and found that catalytic quantities of PL dramatically accelerate the Fe^{3+} and Al^{3+} catalyzed transamination between keto acids and amino acids. The rate acceleration is most pronounced for these specific metals, which happen to be the most abundant in the Earth's crust. Mechanistic studies provide evidence for synergistic catalysis between metal and PL and place the emergence of PLP at an early stage of abiogenesis. This finding is in agreement with conclusions made from cladistic analysis of metabolic pathways,[37] and from in-silico analysis of autocatalytic metabolic networks in LUCA[38,39] or a minimal autotrophic metabolism.[40] Our study constitutes a rare example in which coenzymes are shown to act as catalysts for metabolic reactions in the absence of enzymes and provides a framework for future studies of cooperative effects between metals and coenzymes.

Results and discussion

Baseline reactivity of PL and metal ions. We first studied the transamination of glutamic acid (Glu) with pyruvate (Py) which affords α-ketoglutarate (KG) and alanine (Ala). KG and Py are intermediates of the prebiotically relevant (r)TCA and glyoxylate cycles,[12,41–45] and are two of the universal metabolic precursors to other classes of biomolecules.[46] Glu and Ala are two of the most common prebiotic amino acids.[47] For initial studies, pyridoxal (PL) was chosen over PLP due to its simpler structure, its higher similarity with reported prebiotic syntheses from ammonia and glyceraldehyde,[48] and its greater robustness (Figure S1). However, PL and PLP afforded very similar rates in control experiments (Figure S2). Cu^{2+}, Ni^{2+}, V^{5+}, Fe^{3+}, and Al^{3+} were chosen as primary metal catalysts due to their

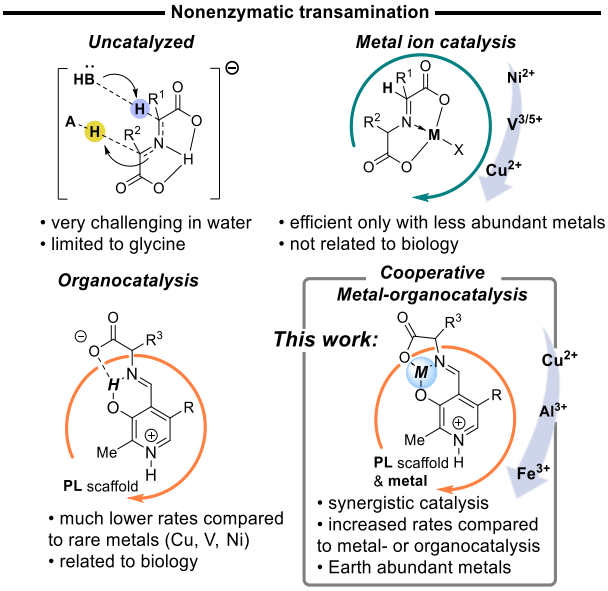

Figure 1. Nonenzymatic transamination systems relevant to prebiotic chemistry (R = CH_2OH or $CH_2OPO_3H^-$).

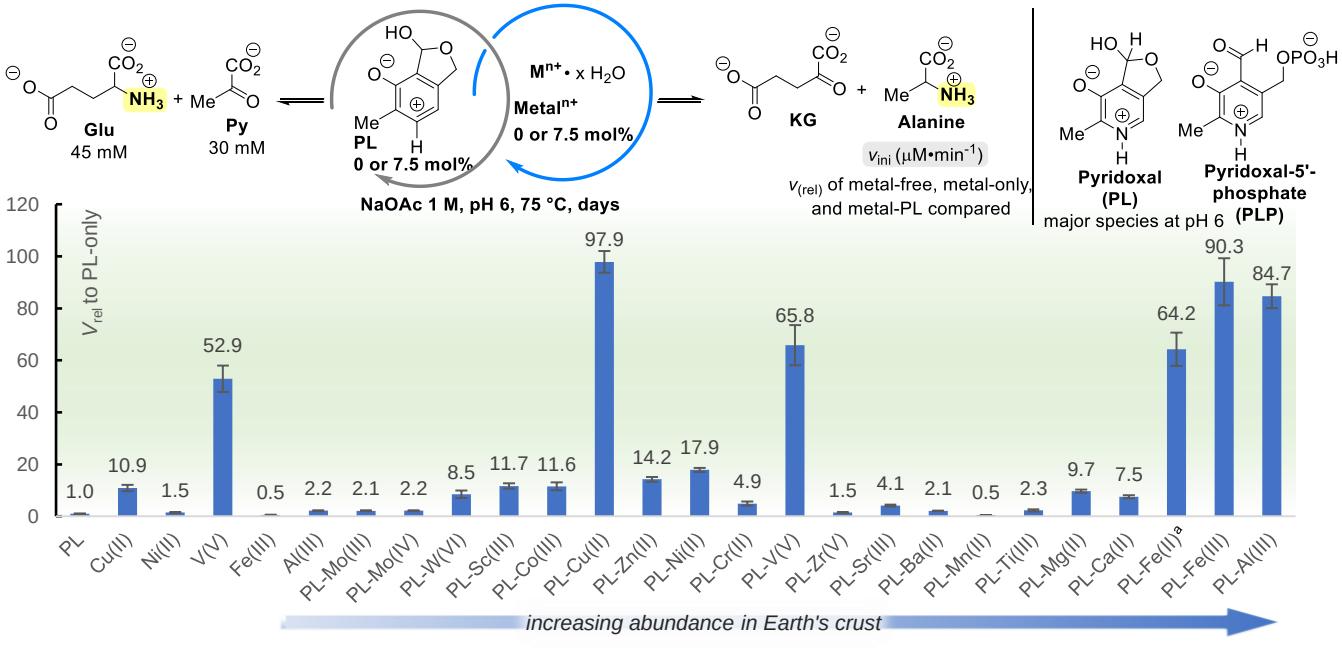

Figure 2. Relative initial rates (v_{rel}) of transamination of glutamic acid to alanine. Conditions: Glu (45 mM), Py (30 mM), PL(P) (0 or 7.5 mol%), metal salt (0 or 7.5 mol%), sodium acetate/acetic acid buffer (1 M, pH 6), 75 °C, 1-7 days. [Ala] determined by calibrated ^{1}H NMR after quenching of aliquots. Initial rates were determined by the slope of the least square linear regression analysis (LR) of time-concentration profiles. Relative rates v_{rel} are expressed relative to metal-free standard conditions with PL (7.5 mol%) and EDTA (3.75 or 7.5 mol%). [a] conducted under inert atmosphere (N_2).

relevance to prebiotic transamination reactions (Cu, Ni, V),[22] their importance in biology (Fe), or their environmental abundance (Fe, Al).[49] The reactions of Glu with Py were studied through the initial rate (v_{ini}) of Ala formation (taken to up to around 10% conversion (based on Py), or, when a more complete reaction profile was obtained, the appropriate linear region). As transamination is under thermodynamic control, a theoretical maximum of 19.4 mM of Ala could form under the chosen conditions.[22] However, as many processes (such as catalyst degradation, product inhibition, reactant/product degradation) can prevent the theoretical equilibrium from being reached, aliquots were subsequently withdrawn every day for a period of 5 to 7 days to record the highest Ala concentration observed ($[Ala]_{max}$) after the determination of initial rates. Studying the reactions of Glu (45 mM) with Py (30 mM) under catalysis from PL (7.5 mol%, 2.25 mM) or from a metal ion (7.5 mol%, 2.25 mM) at pH 6 and 75 °C allowed us to compare the metal-free PL catalysis to the metal-only catalysis in a convenient timeframe. A 1 M acetate buffer was chosen due to the high solubility of metal acetate salts. Reactions were analyzed by ^{1}H NMR after the removal of metals by precipitation at high pH, which resulted in good separation of the characteristic doublet of the Ala -CH_3 resonance. KG and Ala were typically the major products (see the file Supplementary Procedures, Kinetic Data, and DFT Computations (PDF) for details). At this early stage, we learned, as others before us,[24] that PL catalysis is extremely sensitive to trace metal ions. High purity reagents and solvents were needed to ensure reproducible results in metal-free reactions. Furthermore, the metal chelator EDTA was routinely added as an inhibitor of trace metals in metal-free reactions. Under this first set of standard conditions, the comparison of PL-only against metal-only catalysis showed that PL (v_{ini} = 0.77 ± 0.03 μM·min^{-1}, v_{rel} = 1) is significantly outcompeted by simple metal ions (Figure 2). Indeed, the reactions catalyzed by Cu^{2+} (v_{rel} = 10.9 ± 1.2) and V^{5+} (v_{rel} =52.9 ± 5.1) proceeded with significantly higher rates than those catalyzed by PL or PLP. Reactions catalyzed by Ni^{2+} (v_{rel} = 1.5 ± 0.1) and Al^{3+} (v_{rel} = 2.2 ± 0.2) are both faster than Fe^{3+} (v_{rel} = 0.5 ± 0.1). The concentrations of $[Ala]_{max}$ recorded over several days illustrates the consequences of such rate differences: Cu^{2+} and V^{5+} reached [Ala] = 14 mM after 3 and 1 days, respectively, whereas PL only reached [Ala] = 3 mM after more than 5 days (Figure S2). In light of the faster rates provided by Cu^{2+} and V^{5+} ions, it is hard to see the benefit of PL or PLP in the absence of a co-catalyst.

Metal-PL co-catalysis. A complete separation of PL- and metal-catalyzed processes is unlikely under realistic prebiotic conditions. For instance, Fe and Al account for roughly 14% of the Earth's crust, which is a greater portion than all other metals combined. Furthermore, the acidic pH of the early oceans would have favored mineral weathering.[50] Building on earlier research on stoichiometric PL to PM transamination,[24,31,36] we postulated that the presence of metal ions might also be advantageous when using PL in catalytic amounts. Therefore, we systematically screened 18 of the most abundant metals in the Earth's crust and evaluated their effect on PL-catalysis. Monovalent Na^+ and K^+ were found to be catalytically inactive and were thus used as counterions.

Table 1: The effect of buffer and pH on relative rates of PL, metal, and metal-PL catalysis.

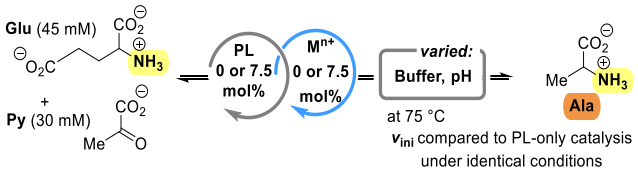

entry	Cat_1	Cat_2	pH	Buffer (M)	v_{ini}[a] (μM/min)	v_{rel}[b] (PL)
1[c]	PL	-	6	NaOAc (1)	0.77	1[c]
2	PL	-	6	NaCl (1)	0.077	1
3	-	Cu^{2+}	6	NaCl (1)	0.34	4
4	-	V^{5+}	6	NaCl (1)	7.65	99
5	-	Fe^{3+}	6	NaCl (1)	0.080	1
6	-	Al^{3+}	6	NaCl (1)	0.25	3
7	PL	Fe^{3+}	7	NaCl (1)	14.9	193
8	PL	Fe^{3+}	6	NaCl (1)	15.8	206
9	PL	Fe^{3+}	5	NaCl (1)	14.6	189
10	PL	Al^{3+}	7	NaCl (1)	14.8	192
11	PL	Al^{3+}	6	NaCl (1)	18.5	240
12	PL	Al^{3+}	5	NaCl (1)	23.7	308
13	PL	-	6	NaPi (0.5)	3.3	1
14	PL	Fe^{3+}	6	NaPi (0.5)	32.2	10
15	PL	Al^{3+}	6	NaPi (0.5)	13.5	4
16	PL	Al^{3+}	6	MES (0.25)	38.6	n.d

Initial rates of alanine formation, catalyzed by PL (0 or 7.5 mol%) and/or metal salts (0 or 7.5 mol%). [a] Initial rates (v_{ini}) were determined by the slope of the least square linear regression analysis of time/concentration profiles determined by ^{1}H NMR after quenching of aliquots. [b] Initial rate relative (v_{rel}) to PL-only catalysis. [c] Metal-free PL data from Figure 2. Pi: pyrophosphate, MES: 2-(*N*-morpholino)ethanesulfonic acid, n.d.: not determined.

Equimolar amounts (7.5 mol%) of PL and metal salts were used in each reaction, and the initial rates (v_{ini}) wererecorded by ^{1}H NMR as before. By plotting the observed rate relative to the rate observed with metal-free PL-catalysis (v_{rel}), two groups of metals were identified as particularly interesting (Figure 2). The first group of metals (Cu^{2+}, Ni^{2+}, V^{5+}) displayed modestly increased rates of catalysis in the presence of PL compared to the PL-only and metal-only controls. Metals in this group were also previously reported as the most active in metal-only catalyzed transamination.[22] In the case of PL + Cu^{2+}, the initial rate was nearly 100-fold faster than with PL alone but was only 10-fold faster than with Cu^{2+} alone. A second group of metals (Fe^{3+}, Al^{3+}), working together with PL, displayed more striking rate acceleration compared to the metal-only catalysis. Metals in this group were not particularly effective in metal-only controls and were highly earth- abundant. The Fe^{3+}-PL system was 90-fold faster than with PL alone and 174-fold than with Fe^{3+} alone. The Al^{3+}-PL system was 85-fold faster than with PL alone and 39-fold faster than with Al^{3+} alone. The $[Ala]_{max}$ observed after 5 to

Table 2: rates of PL and metal-PL catalysis at pH 5

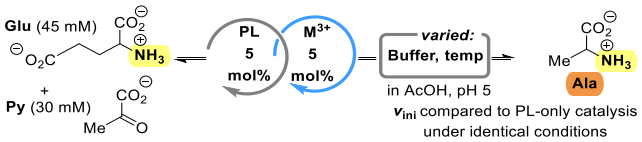

entry	Cat$_1$	Cat$_2$	T (°C)	AcOH (M)	v_{ini}[a] (μM/min)	v_{rel}[b] (PL)
1	PL	-	50	0.25	0.013	1
2	PL	Fe^{3+}	50	0.25	5.22	402
3	PL	Al^{3+}	50	0.25	6.57	496
4	PL	Al^{3+}	35	0.25	2.73[c]	1045[c]
5	PL	Al^{3+}	20	0.25	0.47[c]	NR[d]
6	PL	Al^{3+}	35	1	2.20	307
7	PL	Al^{3+}	20	1	1.04	NR[d]

Initial rates of alanine formation, catalyzed by either PL (5 mol%) and/or metal salts (0 or 5 mol%). [a] Initial rates (v_{ini}) determined by least square linear analysis of time/concentration profiles, determined by ^{1}H NMR after quenching of aliquots. [b] Initial rate relative (v_{rel}) to PL-only catalysis. [c] Reaction conducted with 10 mol% of catalyst(s). [d] No reaction was observed for metal-free PL-catalysis.

7 days were generally consistent with the observed initial rates, apart from Ni^{2+}, which afforded $[Ala]_{max}$ similar to Fe^{3+} (Figure S2). The strong increase in reaction rate for the Fe^{3+}-PL and Al^{3+}-PL systems makes them competitive with Cu^{2+}-PL and V^{5+}-PL. This is particularly important in the prebiotic context, as Fe and Al are the two most abundant metals in Earth's crust (5-6% and 8%, respectively), while Cu and V are relatively scarce (0.006 % and 0.012 %, respectively).[49] These less abundant metals would therefore have been less likely to interact with PL or its analogs in a prebiotic context. Overall, these results show that the PL scaffold is able to amplify the catalytic power of the two most common metals on Earth (Fe, Al) and of rarer metals (Cu, Ni, V), whereas only the latter are capable catalysts on their own.

Buffer effects. We next set out to explore the reactivity landscape of the synergistic Fe^{3+}-PL and Al^{3+}-PL systems under various conditions (Table 1). When the reaction was conducted in saline solution (1 M NaCl) instead of in 1 M acetate/acetic acid buffer, a pH drift of around 0.5 units could be observed, as the reactants and products had a small buffering effect on the reaction. In several instances, at pH values of 5, 6, and 7 and at 75 °C, an even stronger acceleration was found for the metal-PL tandem (entries 7-12) compared to metal or PL alone (entries 2,5,6). Both Fe^{3+}-PL and Al^{3+}-PL exhibited rate accelerations from 189-fold (Fe^{3+}, pH 5, entry 9) to 308-fold (Al^{3+}, pH 5, entry 12) faster than PL-only catalysis. In the saline solution, only the environmentally scarce V^{5+} led to substantial reaction rates (>1 μM·min^{-1}) and yields in the absence of PL co-catalysis (entry 4), highlighting the practical need for co-catalysis with PL on the timeline of life's emergence. Next, we evaluated other buffers that are commonly used by biochemists (phosphate, MES (2-(*N*-morpholino)ethanesulfonic acid), cacodylate, acetate, formate, and lutidine). Buffers are used in studies of prebiotic chemistry to ensure reproducibility and to gain mechanistic insight, although some lack relevance to the early Earth. In addition to controlling the pH, buffers can influence the reaction through general acid-base catalysis (GA-BC) or by coordinating the metal.[51] At a high concentration of 500 mM, phosphate buffer is typically expected to interact strongly with metals, potentially leading to inhibition. Nevertheless, we found that the co-catalyzed reactions still outperformed the metal-free PL reaction (Table 1, entries 14-15). A nitrogen-based buffer, MES, was also compatible with metal-PL catalysis (entry 16). It is clear from these observations that the buffer is not innocent in this reaction: the pH, the buffer pK_a, and the buffer structure all influence the outcome of the reaction in intricate manners. To understand the true influence of pH on the reaction, it is necessary to deconvolute pH effects from buffer effects using a pH-rate analysis.

pH-rate analysis of Al-PL catalysis. Linear correlations between initial rate (v_{ini}) and buffer concentration were observed in four buffers at different pH values that, taken together, cover the pK_a range of 3-7.5. A representative plot is given in Figure 3a, with all plots given in Figure S6. From each of these plots, an initial rate (v^0_{ini}) at a hypothetical zero buffer concentration could be extrapolated and plotted as a function of pH to afford the buffer-independent pH-rate profile shown in Figure 3c. Between pH 3 and 7.5, the profile shows a maximum around pH 6.5, a value consistent with the geochemical environment of the early Earth.[52,53] It should be noted that, in our case, buffers can also influence the outcome of the reaction due to their coordinating abilities. Detailed, quantitative mechanistic analysis of the obtained pH-rate profile is therefore challenging, but it can still be used to illustrate the general behavior of the Al-PL system toward pH, independently of the buffer. Buffers are necessary to ensure reproducibility but often lack prebiotic plausibility and can significantly influence reactions. For example, the buffer-independent rate calculated at pH 5 (v^0_{ini} = 4.9 ± 0.1 μM·min^{-1}) is significantly lower than the one observed in 250 mM acetate buffer at the same pH (v^{250}_{ini} =

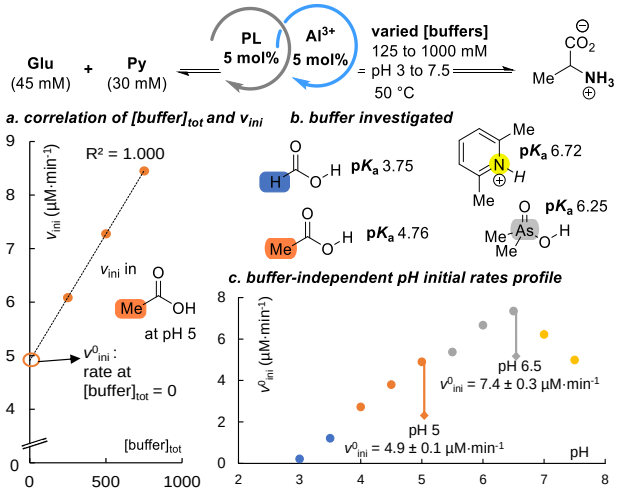

Figure 3. a: correlation between $[buffer]_{tot}$ and initial rates. b: buffers used. c: pH-initial rate profile from the measurement of buffer independent buffer independent initial rates (v^0_{ini}, μM·min^{-1}).

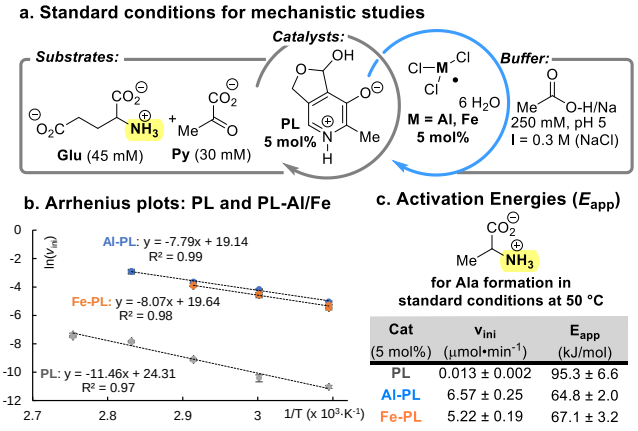

Figure 4. a: Standard conditions used for mechanistic studies. b: Arrhenius plot. c: Apparent activation energies.

6.1 ± 0.1 μM·min^{-1}). Conversely, the buffer-independent rate calculated at pH 7 (v^0_{ini} = 6.0 ± 0.1 μM·min^{-1}) is higher than the observed rate at the same pH in 250 mM lutidine buffer (v^{250}_{ini} = 5.3 ± 0.3 μM·min^{-1}, Table S1). Since buffer effects can serve as mechanistic probes, we searched for conditions suitable for mechanistic analysis.

Identification of conditions suitable for mechanistic studies of metal-PL co-catalysis in transamination. We focused our mechanistic studies on Al^{3+} and Fe^{3+} because their natural abundance is far higher than other active metals. Acetate buffer was chosen due to the prebiotic relevance of carboxylic acids[42] and the linear effect of its concentration on observed rates. A pH of 5 was chosen because it provided ample buffering ability and adequate signal separation in ^{1}H NMR. The loading of PL and the metal co-catalyst was reduced to 5 mol% (1.5 mM), resulting in a metal concentration of roughly 82 ppm for Fe and 40 ppm for Al. Such concentrations are within an order of magnitude of those found in natural water samples.[54] A temperature of 50 °C was chosen as the standard, which is in the range thought to be representative of Earth's mean temperatures in the Hadean era.[52,53] Under these standard conditions, the reaction of Glu (45 mM) with Py (30 mM) produced an even larger rate acceleration compared to PL alone: 400-fold for Fe-PL (Table 2, entry 2) and nearly 500-fold for Al-PL (Table 2, entry 3). At 35 °C, Al-PL was >1000-fold faster than PL alone (Table 2, entry 4). At 20 °C, products could not be observed without metal co-catalysis even after one month (Table 2, entry 5). The effect of PL on metal catalysis was more significant at lower buffer concentrations (see entry 4 vs. entry 6). Finally, we found that the catalysis of transamination by the metal-PL system is not limited to the Glu to Ala transformation. In ^{1}H NMR experiments, we observed significant transamination of glutamate, aspartate, alanine, valine, leucine, *iso*-leucine, serine, and, to a lesser extent, threonine, to glycine at room temperature in less than 48 h under standard conditions (Table S2). These findings emphasize the benefits of metal-PL co-catalysis of transamination under conditions potentially relevant to the origin of the metabolic network.

Arrhenius analysis. An Arrhenius analysis readily explains the temperature effect noted above. Under standard mechanistic conditions (Glu 45 mM, Py 30 mM, PL 5 mol%, Al/Fe 0 or 5 mol%, NaOAc/HOAc 250 mM, pH 5), initial rates (v_{ini}) were recorded between 50 to 90 °C. Plotting ln(v_{ini}) vs. 1/T afforded an Arrhenius plot from which the apparent activation energy (E_{app}) can be calculated (Figure 4b). In multistep mechanisms such as transamination, E_{app} reflects the contributions of all steps exercising a degree of rate control (DRC) on the system.[55] In this way, metal-PL co- catalysis was found to cause a decrease of apparent activation energy E_{app} of around 30 kJ·mol^{-1} for Al-PL (64.8 ± 2.0 kJ·mol^{-1}) and Fe-PL (67.1 ± 3.2 kJ·mol^{-1}) compared to PL-only (95.3 ± 6.6 kJ·mol^{-1}, Figure 4c). This reduction in activation energy causes the relative rate of metal-PL catalysis to increase compared to PL-only catalysis as temperatures decrease, as would be expected for any catalytic pathway offering a lower E_{app}. This effect illustrates how catalysis can favor specific processes over others within more complex reaction networks.[3]

Mechanistic studies. Understanding the synergistic effect of metal-PL catalysis on transamination requires identifying the rate-determining states of the cycle.[56] The energy difference between the resting state (RS) and the rate-determining transition state (RDS) represents the highest barrier to overcome and thus determines the overall kinetics. Transamination catalyzed by aminotransferases follows a *"Ping Pong Bi-Bi"* mechanism, in which two substrates, an amino- and a keto acid, afford two products, their respective keto- and amino acid, with the catalyst shuttling between two unbound states, PL and pyridoxamine (PM). Nonenzymatic PL-catalysis of transamination occurs by a mechanism that follows the same elementary steps.[34] As observed by ^{1}H NMR for the Al-PL

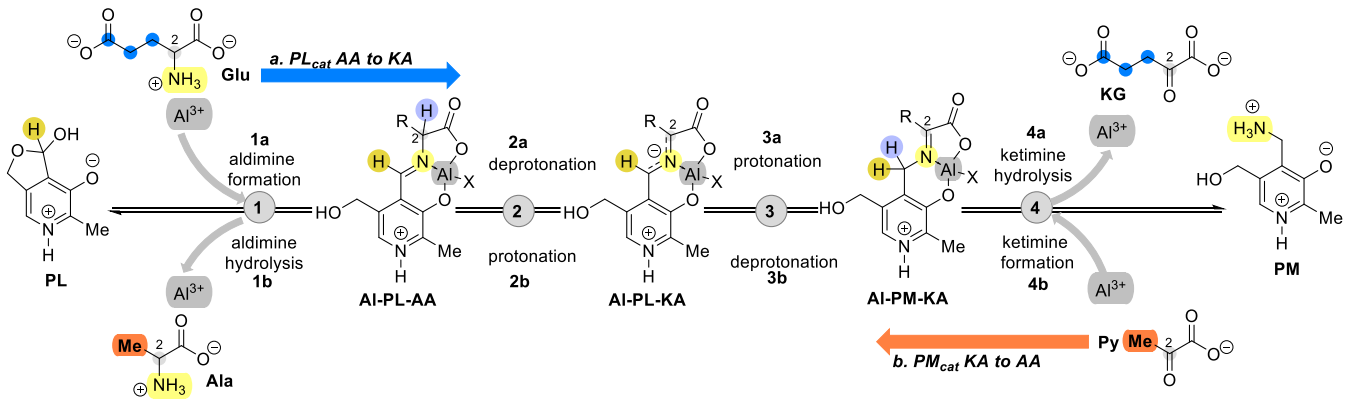

Figure 5. Simplified representation of the catalytic cycle illustrating the key steps of the generally accepted "Ping-Pong Bi-Bi" type mechanism, adapted for Al-PL catalysis (R = $CH_2CH_2COO^-$ or Me).

catalyzed reaction,[57] or in crystal structures of Fe with PL,[58] metals co-catalyze the reaction by forming chelates with the imines formed between PL and amino acids (AA). As Fe^{3+}-PL catalysis led to a complex kinetic profile that furthermore could not be investigated by *in-situ* NMR due to the paramagnetism of Fe^{3+} (Figure S10), we focused our further study on Al-PL catalysis. Because of the symmetry of the process, it is useful to represent the catalytic cycle as a series of identical elementary steps between PL and PM (Figure 5, illustrated with Al^{3+} as metal). From PL, imine formation between the Al and PL catalysts and Glu affords the aldimine Al-PL-Glu (step 1a). Deprotonation of the AA C^2-H position gives the intermediate Al-PL-KG (step 2a), and protonation yields the ketimine Al-PM-KG (step 3a). Finally, hydrolysis provides KG and the Al and PM catalysts (step 4a), which can further react with Py in the reverse order (4b-3b-2b-1b) to provide the second product, Ala, and regenerate the Al and PL catalysts. To start our studies, we first set out to obtain a more complete reaction profile. In our initial investigations, we only monitored Ala formation since, by definition, at least one equivalent of KG must be formed for each equivalent of Ala detected. However, the concentrations of Ala and KG may not be equal at all times since PL must participate in the deamination of Glu, increasing the observed concentration of KG. We first investigated the reaction of Glu (45 mM) with Py (30 mM) at pH 5 (HOAc/NaOAc 250 mM, I = 0.3 M (NaCl)), catalyzed by Al-PL (5 mol%) by *in-situ* ^{1}H NMR at 50 °C (Figure 6). Significant differences in the concentrations of Ala and KG (up to about 0.2 mM) were found at the beginning of the reaction: a short pre-steady state burst of KG formation can be seen, along with a longer induction period for Ala (around 20 min for KG against 50 min for Ala). A steady state was then established

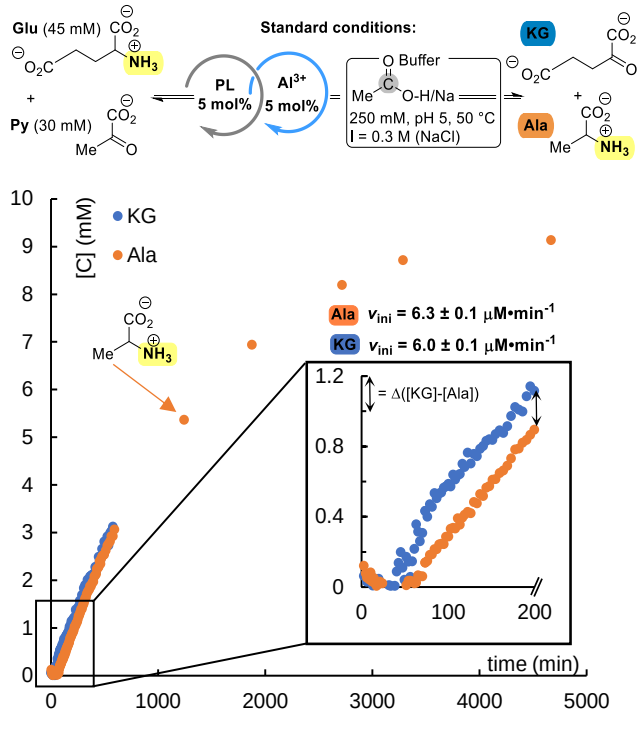

Figure 6. Time-concentration profile of Al-PL catalysis. Initial rates were determined from the time-concentration profiles of three independent in-situ ^{1}H NMR runs by linear regression between 0.2 and 1.5 mM product concentrations.

around [KG] = 0.5 mM and similar rates of formation of KG and Ala were observed for the rest of the time frame studied (up to 600 min), representing roughly 40% conversion (Figure 6). Initial rates measured from three independent runs show v_{ini}^{Ala} = 6.26 ± 0.14 µM·min^{-1} and v_{ini}^{KG} = 6.00 ± 0.12 µM·min^{-1}, in good accordance with the previously obtained value from the manual sampling of the reaction (Table 2, entry 3). Thereafter, only Ala was followed, reaching close to 10 mM concentration after about 5000 min. This reaction profile can be contrasted by the one obtained under identical conditions when Al-pyridoxamine (PM) was used instead of Al-PL as a starting point for catalysis (Figure 7). Here, a larger difference is observed between the rates of formation of Ala vs. KG during the pre-steady state regime (v_{ini}^{Ala} = 19.5 ± 0.9 µM·min^{-1} compared to v_{ini}^{KG} = 5.9 ± 0.2 µM·min^{-1} when measured between 0.02 and 0.5 mM). This difference in the pre-steady state regime explains the significant (≅ 1 mM) difference in the steady state concentrations of [Ala] and [KG] observed when PM is used as the pre-catalyst (Figure 6 and 7, Δ([KG]-[Ala])). More importantly, it shows that the rate-determining states of the catalytic cycle are located in the forward sequence of reactions (i.e., Glu to KG), with the overall rate of the system limited by KG production. Reaction progress kinetic analysis (RPKA) was used to verify whether the Al-PL pair acts as a true catalyst and does not simply modify the equilibrium of the reaction.[59] First, catalyst deactivation was ruled out by performing "same-excess" experiments, where the catalyst is added to a mixture of substrates and products (Glu, Py, KG, and Ala) representative of a reaction at 10% conversion (3 mM).[60] The time profiles of the "same-excess" and standard experiments overlapped, indicating that negligible deactivation or product inhibition occurs (Figure 8a). Next, "different-excess" experiments were conducted.[61] Reactions under standard conditions but with different catalyst loading (Al-PL: 5, 10, and 15 mol%) were performed. As no catalyst deactivation was previously observed, the catalyst concentration was assumed to be constant throughout the runs, allowing for a variable time normalized analysis (VTNA) of the reaction order in Al-PL.[60] The excellent overlay obtained for a partial order of 1 in Al-PL (1:1, denoted as t[Al-PL]^1) over the whole studied timeframe demonstrates that Al-PL is a true catalyst and does not modify the equilibrium constant of the

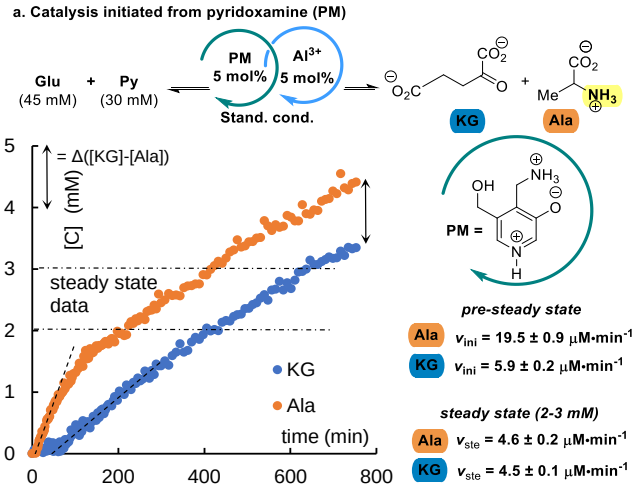

Figure 7: Time-concentration profile of Al-PM catalysis, determined by in-situ ^{1}H NMR. Rates under steady state (v_{ste}) were determined between 2 and 3 mM of Ala.

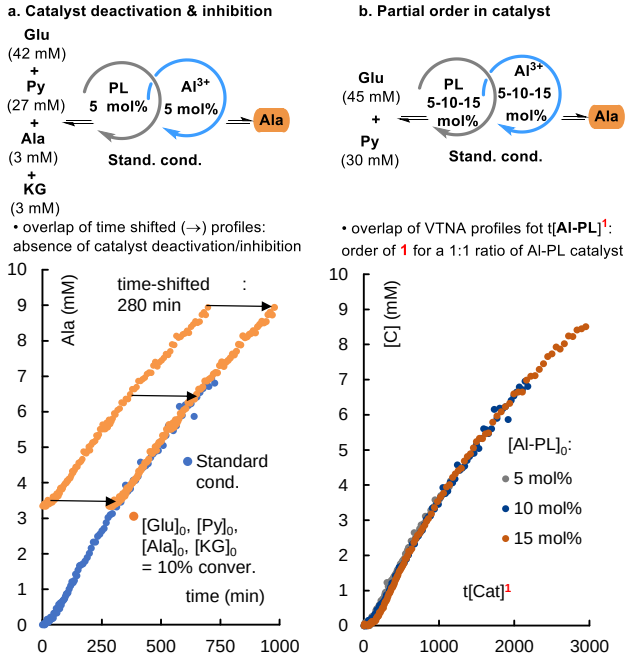

Figure 8. Investigation of the Al-PL catalyst. a: "same-excess" investigation of catalyst deactivation/inhibition. b: VTNA of the reaction order in catalyst, for a partial order of 1 in [Al-PL].

reaction, which otherwise would have resulted in divergent profiles (Figure 8b). The order of 1 also shows that higher-order complexes that have been observed previously[57] and studied here by DOSY, UV, and HRMS (Figure S13-16) are likely not kinetically relevant. Accordingly, the overlaps obtained when performing VTNA using a 1:2 Al/PL ratio (Al = 1.5 mM, PL = 3 mM) for an order of 1 in Al (t[Al]^{1}) and an order of ½ in PL (t[PL]$^{1/2}$) suggests a 1:1 Al-PL complex as the active catalyst (Figure S17).

Kinetic isotope effects. Having established the true catalytic nature of the Al-PL pair and that the rate-determining states are included in the transformation of Glu to KG, we set out to study each step individually. The most convenient step to investigate in the forward direction is arguably step 2, the deprotonation of the C^2-H position of imines derived from Glu. Indeed, kinetic isotope effects (KIE) can readily be evaluated by *in-situ* NMR using DL-glutamic acid-2,4,4-d_3. Thus, KG concentrations were monitored using either Glu (60 mM) or Glu-2,4,4-d_3 (60 mM) under otherwise identical conditions. Figure 9 shows negligible differences in observed KG concentrations. Rates under steady state confirmed the absence of KIE: v^H/v^D = 1.00 ± 0.02. The absence of a KIE indicates that step 2a is not rate determining. Furthermore, for the reaction starting

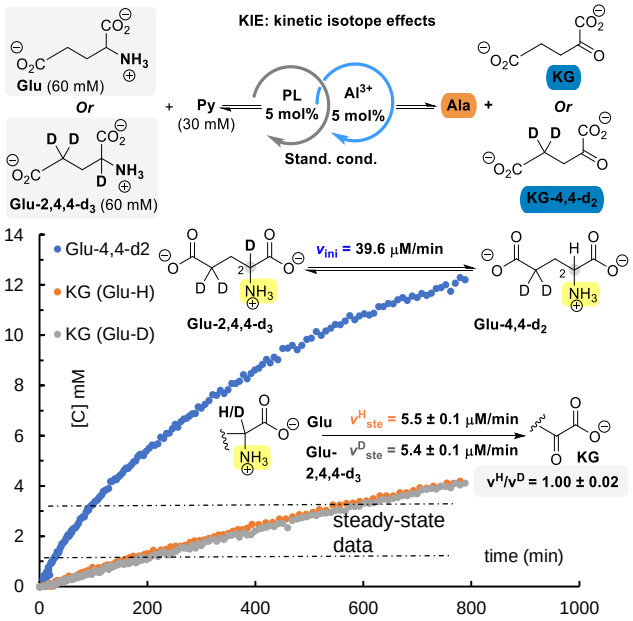

Figure 9. Kinetic isotope effects on KG formation and H/D exchange in Al-PL catalysis. Conditions from Figure 4a, with 60 mM of Glu or Glu-2,4,4-d_3.

from Glu-2,4,4-d_3, we were able to follow the C^2-D D/H exchange velocities by monitoring the formation of Glu-4,4-d_2. The much higher concentrations and observed rates of Glu-4,4-d_2 formation compared to downstream products ($v_{ini}^{Glu\text{-}d2}$ = 39.6 ± 1.3 μM·min^{-1}) indicate the highly reversible character of step 1 and step 2, and thus neither can be rate-limiting. Identical v^H/v^D values were found when Ala formation was monitored under the same conditions (Figure S18). KIE were also determined at other pH values by the method of initial rates (following [Ala]): KIEs very close to 1 were observed at pH 4 (v_{ini}^H/v_{ini}^D = 0.96 ± 0.04) and pH 6 (v_{ini}^H/v_{ini}^D = 1.08 ± 0.03). These results demonstrate that neither step 1, imine formation, nor step 2, deprotonation, can be rate-limiting. The RDS for the Al-PL catalyzed reaction is, therefore, different than the RDS for the metal-free PL catalyzed reactions, where strong primary KIEs were reported in the stoichiometric transamination of PL to PM under pseudo-first order conditions (k_H/k_D > 2).[33,62] This change in RDS is likely due to the acidification of the C^2-H proton under Al complexation (Figure S19). A parallel can also be made with enzymatic transamination, although the interpretation is more complex. For instance, the significant KIEs (k_H/k_D ~ 2)[63,64] reported for several aspartate transaminases were later interpreted as being part of a multi-RDS mechanism,[65] a situation where enzymes are optimized by evolution to achieve similar reaction barriers across a catalytic cycle.[66]

Investigation of the resting state. Two steps might potentially be rate-determining: step 3a, protonation, and step 4a, hydrolysis. Occurring further down the catalytic path, they can be investigated through their effect on the overall kinetics, which requires identifying the catalytic resting state. We thus studied the species in solution across four independent reactions (three reactions initiated from Al-PL, one reaction initiated from Al-PM) to determine their mean concentrations at steady state. Representative ^{1}H NMR spectra are shown in Figure 10. At pH 5, the species

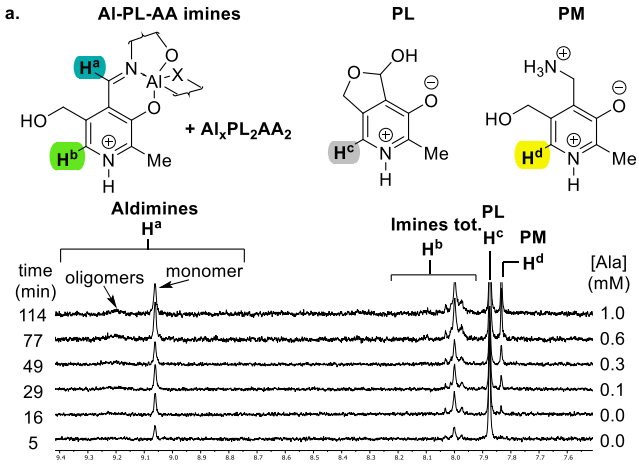

b. Species repartition under steady state

[PL]	[PM]	[Imine]$_{total}$	[Ketimine]	[Aldimine]
41% (1)	21% (2)	37% (2)	21% (4)	16% (5)

Figure 10. a: Representative evolution of catalyst species under standard conditions when followed by ^{1}H NMR. b: Species repartition under steady state with [PL]+[PM]+[Imines]$_{tot}$ = 100%. The standard deviation over four independent runs is given in parentheses.

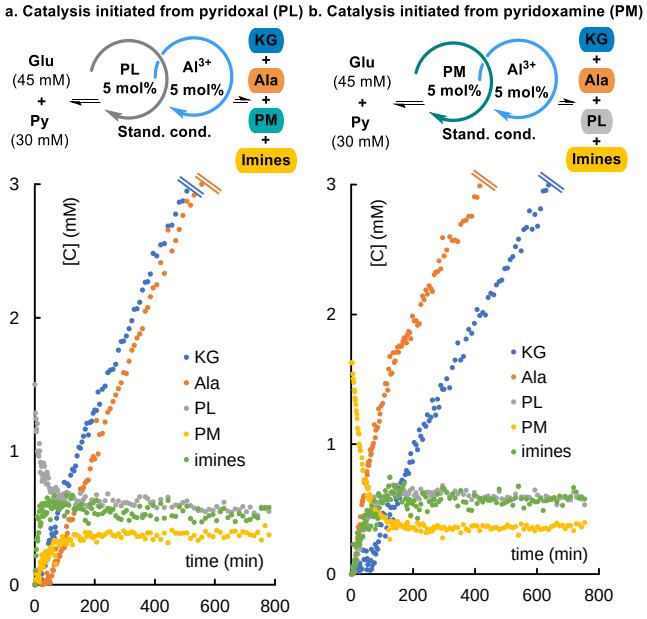

Figure 11. Investigation of the resting state of the catalyst under standard conditions, followed by ^{1}H NMR. a: Concentration when initiating the reaction from Al-PL. b: Concentrations when initiating the reaction from Al-PM.

distribution at steady state was found to be 41% PL, 21% PM, and 37% Al-imine complexes (corresponding to 21% aldimines and 16% ketimines). Among the Al-imine complexes, the kinetically relevant monomeric complex (1:1:1 Al-PL-Glu) is the major species, with oligomeric aldimine complexes ($Al_xPL_2AA_2$) accounting for 10-20% of the species depending on the pH and buffer environment. Further quantitative determination of all present imines was not possible due to the high number of species and peak overlap. As PL is the major species (41%), and because we have shown that PL is in fast equilibrium with the aldimines, a portion of the 21% of aldimines must be involved in the PL ⇋ Al-PL-Glu equilibrium. Thus, we can conclude that the species involved in the PL ⇋ Al-PL-Glu equilibrium comprise the resting state of the catalyst. The PL ⇋ Al-PL-Glu equilibrium as the catalyst resting state is illustrated by two time-concentration profiles in Figure 11, where concentrations of the catalytic species have been added to the data presented in Figures 6 and 7. Starting the catalysis from PL, the rate of $[Im]_{tot}$ formation is closely related to the rate of PL disappearance (Figure 11a). Starting from PM, the rate of $[Im]_{tot}$ formation was found to be closely related to the rate of PL formation (Figure 11b), further confirming the fast equilibrium between PL and its imines. We note that the deprotonated intermediate Al-PL-KA, previously identified in stoichiometric Al-PL to Al-PM reactions,[67] was not detected under our catalytic conditions. Taking into account the proposed resting state, the reaction should therefore follow pre-equilibrium approximation kinetics, with rapid and reversible step(s) 1a and 2a (Figure 5) preceding the limiting step(s). Thus, imine formation (step 1), despite not being rate-limiting, would still influence kinetics by regulating the imine available in the subsequent slow step(s).[68] Such pre-equilibrium kinetics are consistent with previous UV-Vis studies on the stoichiometric half-reaction of PL to PM in the presence of excess Al^{3+}, where it was proposed that Al^{3+} increases rates by increasing imine concentration.[36]

Investigation of the RDS. The concentrations observed under steady state suggest that step 4a, ketimine hydrolysis, is the RDS, as only traces of the deprotonated intermediate of step 3a were detected. However, the ketimines could not be isolated and studied directly because they rapidly tautomerize to aldimines, which are 17 kJ·mol^{-1} more stable by DFT calculations (Figure S20). We therefore chose to study the RDS indirectly through the influence of acids and bases on the overall catalysis. For example, at pH 5-6, the two potentially rate-limiting steps, protonation and imine hydrolysis, should be susceptible to general acid catalysis (GAC)[28] and general base catalysis (GBC),[69] respectively (Figure 12a). Probing which mechanism, GAC or GBC, increases the rate can, therefore, inform us of the RDS. To do so, we first established that GAC or GBC were operative in the Al-PL system and then showed that the considered RDS is indeed accelerated by GA-BC. The influence of buffer concentration ($[buffer]_{tot}$) on the initial rate was surveyed over the pH range 3-7.5 using four different buffers (see Figure 12b for runs at a buffer concentration of 250 mM). The linear correlation observed in Figure 12c between v_{ini} and $[buffer]_{tot}$ at several pH values is characteristic of buffer catalysis through GAC or GBC.[51] Figure 12c also strongly suggests that the Al-PL system is more susceptible to base catalysis than to acid catalysis: First, at a constant buffer concentration, v_{ini} increases with increasing pH across several buffers (at $[buffer]_{tot}$ = 250 mM: entry 1 to 8, Figure 12b). Second, when comparing two different buffers at pH 5.5 (cacodylate and acetate, Figure 12c), the buffer with the higher pK_a (cacodylate) shows higher rates. Third, when the cacodylate buffer is compared at pH 5.5 and 6.5 (Figure 12c), higher rates and a steeper linear dependence are observed in the latter case, where more cacodylate

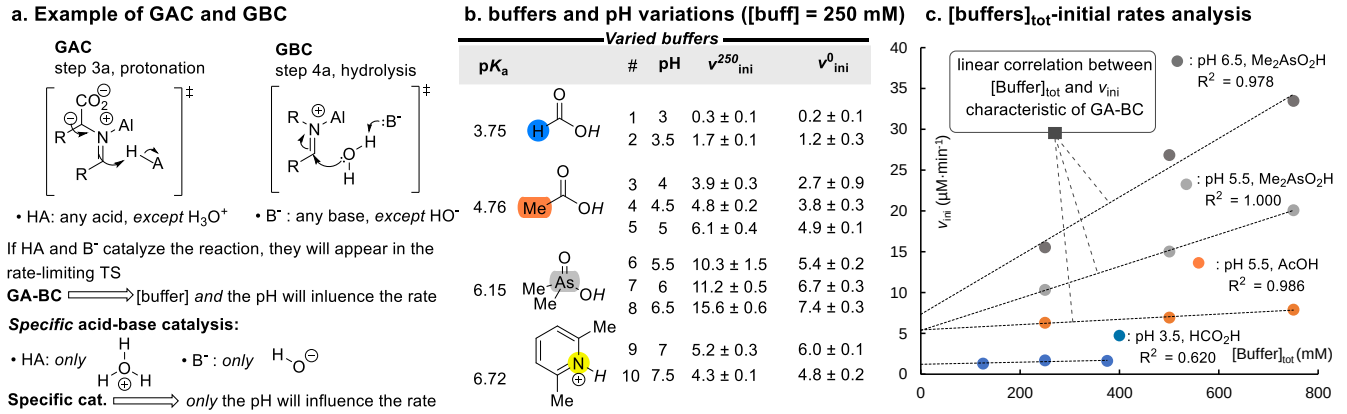

Figure 12. pH- and buffer-rate measurements in the investigation of the RDS. a: Illustration of the mechanism of general acid catalysis (GAC) and general base catalysis (GBC). b: Initial rates measurement in 250 mM of the stated buffers (v^{250}_{ini}) at different pH values. Extrapolated initial rates at zero buffer concentration (v^{0}_{ini}) are determined from the intercept of a least-square linear regression analysis of the [buffer]$_{tot}$-pH profile (the ionic strength was maintained at I ≥ 0.3 with NaCl). c: Initial rates of Ala formation in different buffers at different pH values, with least-square linear regression of rates vs. [buffer] total concentration at the stated pH values. All rates are expressed in μM·min^{-1}.

anion is present in solution. Finally, higher intercepts of the linear regression analysis are found at higher pH values. These intercepts represent the rate extrapolated to zero buffer concentration (v^{0}_{ini}), which are the rates of the reaction catalyzed by, specifically, H^+ and OH^- (i.e specific acid-base catalysis).[70]

Investigation of the resting state in Me$_2$AsOOH buffer. The strong influence of base catalysis on the Al-PL system indicates that imine hydrolysis is the most likely RDS. To confirm this interpretation, we first ruled out that the increased rates simply resulted from an increase in the concentration of the catalytically active imine (Figure 13). On the contrary, following the kinetics in Me$_2$AsOO-H/Na buffer, which afforded higher rates than acetate buffer (v^{As}_{ini} =12.4 μM·min^{-1} vs. v^{Ac}_{ini} = 6.6 μM·min^{-1}), indicated a decrease in imine concentration (13% vs. 37% in acetate buffer), as well as an increase in PL concentration (60% vs. 44% in acetate buffer) and little change in PM concentration (26% vs. 23% in acetate buffer) at steady state. These

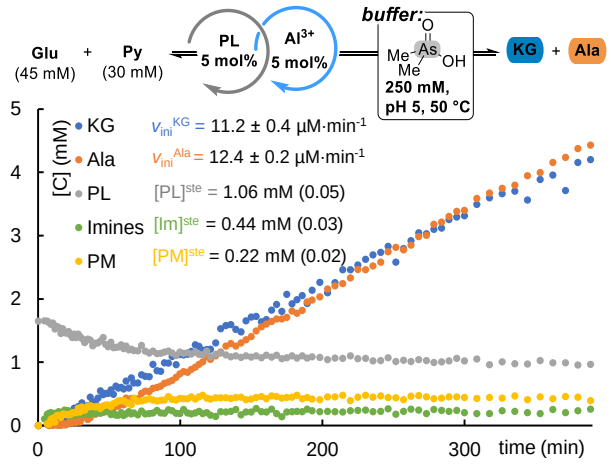

Figure 13. Time-profile of Al-PL catalysis in Me$_2$AsOOH buffer (pH 5, 250 mM). Initial rates (v_{ini}) were determined between 0.5 and 1.5 mM. Mean steady-state concentrations [C]^{ste} are shown between 100-400 min, with standard deviations in parentheses.

findings are consistent with a PL resting state and rate-limiting imine hydrolysis in the conversion of Glu to KG.

Imine hydrolysis in Me$_2$AsOOH buffer monitored by UV-Vis spectroscopy. To confirm that buffers with higher pK_a values accelerate the overall reaction by increasing the rates of hydrolysis of the Al-PL imines through GBC catalysis, we studied the relevant imines. As previously noted, the substantial thermodynamic preference for the aldimine tautomer and the fast interconversion between aldimines and ketimines does not allow the direct study of the ketimine species. We therefore prepared and isolated the Al-PL-Glu and metal-free PL-Glu aldimines and studied them by UV-Vis spectroscopy, monitoring the pseudo-first order disappearance of their characteristic Schiff base absorbance in acetate and cacodylate buffers. Representative kinetic runs are shown in Figure 14. The increased stability of the metalated imine was evident, with Al-PL-Glu hydrolyzing 259-fold slower than PL-Glu in acetate buffer (250 mM, pH 5, I = 0.3 (NaCl)). The hydrolysis of Al-PL-Glu was found to be 2.4-fold faster in the higher pK_a cacodylate buffer compared to acetate buffer (both at pH 5 and 250 mM), a difference similar to that observed for the full catalytic transformation when carried out in those two buffers. We confirmed that this effect is due to buffer catalysis by performing the comparison at several buffer concentrations (Figure S22). This result highlights the importance of general base catalysis in the hydrolysis of metalated imines, a step that releases the product. The result also confirms that imine hydrolysis, as the product-releasing RDS, and imine formation, which increases the concentration of the active catalyst, are both capable of influencing the rate of the Al-PL catalyzed reaction.

Evolutionary considerations. The importance of GA-BC and the rate-limiting ketimine hydrolysis in metal-PL catalyzed transamination draws interesting parallels with biology and suggests a hypothesis for the molecular evolution of transamination chemistry. Indeed, the substantial rate acceleration observed in metal-PL co-catalysis compared to metal-only or PL-only catalysis raises the possibility of an intermediary stage between metal-only

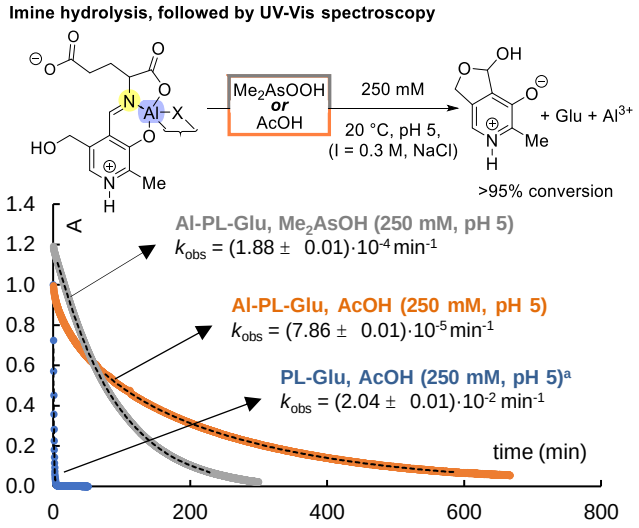

Figure 14. Pseudo-first order rate constants (k_{obs}) of aldimine hydrolysis measured by the decrease of the Al-PL-Glu absorbance at 370 nm. [a] Decrease followed at an absorbance of 410 nm and normalized to 1

and enzyme-PL catalysis. Several mechanistic traits are common between metal-PL catalysis and biological transamination. First, the susceptibility of the Al-PL system to GBC recapitulates prior direct observations of GBC in PLP-dependent transaminases with exogenous amines.[71] GA-BC is one of the major mechanisms by which enzymes increase reaction rates.[51] Second, as for the Al-PL catalyst, mutant transaminases in which a single tyrosine residue is missing from the active site also display a kinetic profile implicating ketimine hydrolysis as the RDS.[72] It is therefore conceivable that the metal center in metal-PL systems could have pre-organized early metal-PL-peptide systems, allowing further improvement of reaction rates by GA-BC. Why, then, did nature eventually choose to optimize its enzymes for a metal-free transamination rather than one co-catalyzed by metals? Our mechanistic findings provide a potential answer. Working together with PLP, metals allow significant catalyst concentrations to be achieved in water and facilitate deprotonation of the imine intermediate. However, the superior substrate binding is necessarily counteracted by more challenging product release. Product dissociation is often one of the most difficult steps to optimize under enzyme catalysis.[66,73] The global maximum for the optimization of enzymatic transamination is, therefore, more likely to be found in a reaction without metals. Strong metal chelation also reduces the attainable conformations in the active site, a limitation not found in present-day transaminases. PLP-dependent enzymes of the same evolutionary origin as transaminases also catalyze reactions beyond transamination, a versatility that is directly related to the free orientation of the bonds at the C^2-AA carbon.[74,75] Such conformational freedom would be restricted in metal-PL systems.

Conclusions

In summary, PL and metals exhibit a synergistic effect on the catalysis of transamination of amino acids and keto acids. The combination of PL with the two most common metals on Earth, Fe and Al, provides the greatest accelerations. Metal loadings of Al^{3+} up to 2000-fold lower than its content in the Earth's crust provided up to 1000-fold rate acceleration compared to the same reaction in the absence of metal. The co-catalytic system was effective in a wide range of pH (4-7.5), temperatures (20-75 °C), and buffers. Less abundant metal ions that were previously found to be effective catalysts for transamination in the absence of PL (Cu^{2+}, V^{5+}) are also substantially accelerated by its presence, though to a lesser extent than Fe^{3+} and Al^{3+}.

Experimental and theoretical mechanistic studies indicate that the rate-determining step in the PL-metal-catalyzed transamination is different from metal-free and biological PL-based catalysis. Metal coordination to PL lowers the pK_a of the PL-metal complex by several units and slows the imine intermediate's hydrolysis by up to 259-fold. The formation of a metal PL-imine chelate serves to increase the active catalyst concentration. The PL-metal system is susceptible to general acid-base catalysis and was found to follow the Ping-Pong Bi-Bi mechanism, both characteristic of the PL-enzyme system.

This work constitutes a rare example in which coenzymes are shown to act as effective catalysts for metabolic reactions in the absence of enzymes. In the context of the origin of metabolism, this direct chemical evidence is consistent with diverse other findings suggesting an early emergence of PL(P) before enzymes.[37–40] In one of several possible evolutionary trajectories, transamination may have initially been catalyzed by rare metal ions such as Cu^{2+} or V^{5+} in localized environments enriched in such metals. However, the production of PL(P) by a protometabolism would allow highly abundant metals such as Fe^{3+} and Al^{3+} to take over this function, releasing the dependence of the protometabolism on niche inorganics and allowing it to spread to more ubiquitous environments. Profiling the metal dependence of other coenzymes with respect to their nonenzymatic activity in fundamental biological reactions may give insight into the environment in which protometabolism first emerged.

ASSOCIATED CONTENT

Supporting Information. The Supporting Information is available free of charge on the ACS Publications website. Supplementary figures and tables, detailed experimental procedures, kinetics data and ^{1}H NMR data, UV-Vis studies procedures and results, *in-situ* NMR data and RPKA analysis; computational procedures, results, and atoms coordinates (file Supplementary Information, PDF).

AUTHOR INFORMATION

Corresponding Author

*q.dherbassy@unistra.fr, *moran@unistra.fr

ACKNOWLEDGMENT

This project has received funding from the European Research Council (ERC) under the European Union's Horizon 2020 research and innovation programme (grant agreement n° 101001752). The work was also supported by the Interdisciplinary Thematic Institute ITI-CSC via the IdEx Unistra (ANR-10-IDEX-0002) within the program Investissement d'Avenir. J.M. thanks the VW Foundation (no. 96_742) for generous support. R.J.M. thanks the Deutsche Forschungsgemeinschaft (DFG, German Research Foundation) for a fellowship (MA 9687/1-1). Computations were performed at the High Performance Computing Center of the University of Strasbourg. Part of the computing resources were funded by the Equipex Equip@Meso project (Programme Investissements d'Avenir).

ABBREVIATIONS

PLP, pyridoxal-5'-phosphate; PL, pyridoxal; PMP, pyridoxamine-5'-phosphate; PM, pyridoxamine; AA, amino acid; KA, keto acid; Glu, glutamic acid; Py, pyruvate; KG, α-ketoglutarate; Ala, alanine; LR, least-square linear regression; STE, steady state; TS, transition state; DRC, degree of rate control; RDS, rate-determining states; RPKA, reaction progress kinetic analysis; VTNA, variable time normalization analysis. GA-BC, general acid-base catalysis; GAC, general acid catalysis; GBC general base catalysis.

REFERENCES

(1) Smith, E.; Morowitz, H. J. The Autotrophic Origins Paradigm and Small-Molecule Organocatalysis. *Orig Life Evol Biosphere* **2010**, *40*, 397–402. https://doi.org/10.1007/s11084-010-9213-2.

(2) Szöke, A.; Scott, W. G.; Hajdu, J. Catalysis, Evolution and Life. *FEBS Lett.* **2003**, *553* (1–2), 18–20. https://doi.org/10.1016/S0014-5793(03)01008-1.

(3) Pascal, R. Kinetic Barriers and the Self-Organization of Life. *Isr. J. Chem.* **2015**, *55* (8), 865–874. https://doi.org/10.1002/ijch.201400193.

(4) Muchowska, K. B.; Varma, S. J.; Moran, J. Nonenzymatic Metabolic Reactions and Life's Origins. *Chem. Rev.* **2020**, *120* (15), 7708–7744. https://doi.org/10.1021/acs.chemrev.0c00191.

(5) Graaf, R. de; Sojo, V.; Hudson, R. Catalysis at the Origin of Life. ChemRxiv July 1, 2022. https://doi.org/10.26434/chemrxiv-2022-xhmzj.

(6) Camprubi, E.; Jordan, S. F.; Vasiliadou, R.; Lane, N. Iron Catalysis at the Origin of Life. *IUBMB Life* **2017**, *69* (6), 373–381. https://doi.org/10.1002/iub.1632.

(7) White, H. B. Coenzymes as Fossils of an Earlier Metabolic State. *J. Mol. Evol.* **1976**, *7* (2), 101–104. https://doi.org/10.1007/BF01732468.

(8) Chu, X.-Y.; Zhang, H.-Y. Cofactors as Molecular Fossils To Trace the Origin and Evolution of Proteins. *ChemBioChem* **2020**, *21* (22), 3161–3168. https://doi.org/10.1002/cbic.202000027.

(9) Weiss, M. C.; Sousa, F. L.; Mrnjavac, N.; Neukirchen, S.; Roettger, M.; Nelson-Sathi, S.; Martin, W. F. The Physiology and Habitat of the Last Universal Common Ancestor. *Nat. Microbiol.* **2016**, *1* (9), 1–8. https://doi.org/10.1038/nmicrobiol.2016.116.

(10) Ribeiro, A. J. M.; Holliday, G. L.; Furnham, N.; Tyzack, J. D.; Ferris, K.; Thornton, J. M. Mechanism and Catalytic Site Atlas (M-CSA): A Database of Enzyme Reaction Mechanisms and Active Sites. *Nucleic Acids Res.* **2018**, *46* (D1), D618–D623. https://doi.org/10.1093/nar/gkx1012.

(11) Mukhopadhyay, A.; Borkakoti, N.; Pravda, L.; Tyzack, J. D.; Thornton, J. M.; Velankar, S. Finding Enzyme Cofactors in Protein Data Bank. *Bioinformatics* **2019**, *35* (18), 3510–3511. https://doi.org/10.1093/bioinformatics/btz115.

(12) Muchowska, K. B.; Varma, S. J.; Moran, J. Synthesis and Breakdown of Universal Metabolic Precursors Promoted by Iron. *Nature* **2019**, *569* (7754), 104–107. https://doi.org/10.1038/s41586-019-1151-1.

(13) King, G. A. M. Evolution of the Coenzymes. *Biosystems* **1980**, *13* (1), 23–45. https://doi.org/10.1016/0303-2647(80)90003-9.

(14) Vella, F. Beginnings of Cellular Life: Metabolism Recapitulates Biogenesis: By H J Morowitz. Pp. 195. Yale University Press, New Haven and London. 1992. *Biochem. Educ.* **1994**, *22* (2), 109–109. https://doi.org/10.1016/0307-4412(94)90116-3.

(15) Xavier, J. C.; Kauffman, S. Small-Molecule Autocatalytic Networks Are Universal Metabolic Fossils. *Philos. Trans. R. Soc. Math. Phys. Eng. Sci.* **2022**, *380* (2227), 20210244. https://doi.org/10.1098/rsta.2021.0244.

(16) Kirschning, A. Coenzymes and Their Role in the Evolution of Life. *Angew. Chem. Int. Ed.* **2021**, *60* (12), 6242–6269. https://doi.org/10.1002/anie.201914786.

(17) Percudani, R.; Peracchi, A. A Genomic Overview of Pyridoxal-Phosphate-Dependent Enzymes. *EMBO Rep.* **2003**, *4* (9), 850–854. https://doi.org/10.1038/sj.embor.embor914.

(18) Eliot, A. C.; Kirsch, J. F. Pyridoxal Phosphate Enzymes: Mechanistic, Structural, and Evolutionary Considerations. *Annu. Rev. Biochem.* **2004**, *73* (1), 383–415. https://doi.org/10.1146/annurev.biochem.73.011303.074021.

(19) Mueser, T. C.; Drago, V.; Kovalevsky, A.; Dajnowicz, S. Chapter Fifteen - Pyridoxal 5′-Phosphate Dependent Reactions: Analyzing the Mechanism of Aspartate Aminotransferase. In *Methods in Enzymology*; Moody, P. C. E., Ed.; Neutron Crystallography in Structural Biology; Academic Press, 2020; Vol. 634, pp 333–359. https://doi.org/10.1016/bs.mie.2020.01.009.

(20) Nakada, H. I.; Weinhouse, S. NON-ENZYMATIC TRANSAMINATION WITH GLYOXYLIC ACID AND VARIOUS AMINO ACIDS. *J. Biol. Chem.* **1953**, *204* (2), 831–836. https://doi.org/10.1016/S0021-9258(18)66086-7.

(21) Mix, H. Nichtenzymatische Transaminierung Zwischen α-Aminosäuren und α-Ketosäuren in Gegenwart von Metallionen. *Hoppe Seylers Z. Physiol. Chem.* **1959**, *315*, 1–12. https://doi.org/10.1515/bchm2.1959.315.1.1.

(22) Mayer, R. J.; Kaur, H.; Rauscher, S. A.; Moran, J. Mechanistic Insight into Metal Ion-Catalyzed Transamination. *J. Am. Chem. Soc.* **2021**, *143* (45), 19099–19111. https://doi.org/10.1021/jacs.1c08535.

(23) Snell, E. E. The Vitamin B_6 Group. V. The Reversible Interconversion of Pyridoxal and Pyridoxamine by Transamination Reactions. *J. Am. Chem. Soc.* **1945**, *67* (2), 194–197. https://doi.org/10.1021/ja01218a013.

(24) Metzler, D. E.; Snell, E. E. Some Transamination Reactions Involving Vitamin B_6 [1]. *J. Am. Chem. Soc.* **1952**, *74* (4), 979–983. https://doi.org/10.1021/ja01124a033.

(25) Metzler, D. E.; Olivard, J.; Snell, E. E. Transamination of Pyridoxamine and Amino Acids with Glyoxylic Acid1. *J. Am. Chem. Soc.* **1954**, *76* (3), 644–648. https://doi.org/10.1021/ja01632a003.

(26) Bruice, T. C.; Topping, M. Catalytic Reactions Involving Azomethines. I. The Imidazole Catalysis of the Transamination of Pyridoxal by α-Aminophenylacetic Acidla. **1963**, *85*, 1480–1488.

(27) Bruice, T. C.; Topping, M. Catalytic Reactions Involving Azomethines. II. The PH Dependence of the Imidazole Catalysis of the Transamination of Pyridoxal by α-Aminophenylacetic Acid. *J. Am. Chem. Soc.* **1963**, *85* (10), 1488–1493. https://doi.org/10.1021/ja00893a023.

(28) Bruice, T. C.; Topping, R. M. Catalytic Reactions Involving Azomethines. III.1 The Influence of Morpholine upon the Imidazole Catalysis of the Transamination of Pyridoxal by α-Aminophenylacetic Acid. The Transamination of the Morpholine Imine of Pyridoxal. *J. Am. Chem. Soc.* **1963**, *85* (10), 1493–1496. https://doi.org/10.1021/ja00893a024.

(29) French, T. C.; Bruice, T. C. Catalytic Reactions Involving Azomethines. IV. * Rates and Equilibria of Imine Formation with Pyridine-4-Aldehyde and Various Amino Acids. *Biochemistry* **1964**, *3* (10), 1589–1596. https://doi.org/10.1021/bi00898a035.

(30) French, T. C.; Auld, D. S.; Bruice, T. C. Catalytic Reactions Involving Azomethines. V. Rates and Equilibria of Imine Formation with 3-Hydroxypyridine-4-Aldehyde and Amino Acids*. *Biochemistry* **1965**, *4* (1), 77–84. https://doi.org/10.1021/bi00877a014.

(31) Thanassi, J. W.; Butler, A. R.; Bruice, T. C. Catalytic Reactions Involving Azomethines. VI. The Mechanism of the Transamination of 3-Hydroxypyridine-4-Aldehyde by Glutamic Acid *. *Biochemistry* **1965**, *4* (8), 1463–1472. https://doi.org/10.1021/bi00884a001.

(32) Auld, D. S.; Bruice, T. C. Catalytic Reactions Involving Azomethines. VII.[1] Rates and Equilibria of Aldimine Formation with 3-Hydroxypyridine-4-Aldehyde and Alanine. *J. Am. Chem. Soc.* **1967**, *89* (9), 2083–2089. https://doi.org/10.1021/ja00985a020.

(33) Auld, D. S.; Bruice, T. C. Catalytic Reactions Involving Azomethines. VIII.[1] Water and Alanine Catalysis of the Transamination of 3-Hydroxypyridine-4-Aldehyde by Alanine. *J. Am. Chem. Soc.* **1967**, *89* (9), 2090–2097. https://doi.org/10.1021/ja00985a021.

(34) Auld, D. S.; Bruice, T. C. Catalytic Reactions Involving Azomethines. IX.[1] General Base Catalysis of the Transamination of 3-Hydroxypyridine-4-Aldehyde by Alanine. *J. Am. Chem. Soc.* **1967**, *89* (9), 2098–2106. https://doi.org/10.1021/ja00985a022.

(35) Longenecker, J. B.; Snell, E. E. The Comparative Activities of Metal Ions in Promoting Pyridoxal-Catalyzed Reactions of Amino Acids[1]. *J. Am. Chem. Soc.* **1957**, *79* (1), 142–145. https://doi.org/10.1021/ja01558a036.

(36) Zabinski, R. F.; Toney, M. D. Metal Ion Inhibition of Nonenzymatic Pyridoxal Phosphate Catalyzed Decarboxylation and Transamination. *J. Am. Chem. Soc.* **2001**, *123* (2), 193–198. https://doi.org/10.1021/ja0026354.

(37) Cunchillos, C.; Lecointre, G. Evolution of Amino Acid Metabolism Inferred through Cladistic Analysis. *J. Biol. Chem.* **2003**, *278* (48), 47960–47970. https://doi.org/10.1074/jbc.M213028200.

(38) Xavier, J. C.; Hordijk, W.; Kauffman, S.; Steel, M.; Martin, W. F. Autocatalytic Chemical Networks at the Origin of Metabolism. *Proc. R. Soc. B Biol. Sci.* **2020**, *287* (1922). https://doi.org/10.1098/rspb.2019.2377.

(39) Wimmer, J. L. E.; Vieira, A. do N.; Xavier, J. C.; Kleinermanns, K.; Martin, W. F.; Preiner, M. The Autotrophic Core: An Ancient Network of 404 Reactions Converts H_2, CO_2, and NH_3 into Amino Acids, Bases, and Cofactors. *Microorganisms* **2021**, *9* (2), 458. https://doi.org/10.3390/microorganisms9020458.

(40) Martin, W.; Russell, M. J. On the Origin of Biochemistry at an Alkaline Hydrothermal Vent. *Philos. Trans. R. Soc. B Biol. Sci.* **2007**, *362* (1486), 1887–1926. https://doi.org/10.1098/rstb.2006.1881.

(41) Muchowska, K. B.; Varma, S. J.; Chevallot-Beroux, E.; Lethuillier-Karl, L.; Li, G.; Moran, J. Metals Promote Sequences of the Reverse Krebs Cycle. *Nat. Ecol. Evol.* **2017**, *1* (11), 1716–1721. https://doi.org/10.1038/s41559-017-0311-7.

(42) Varma, S. J.; Muchowska, K. B.; Chatelain, P.; Moran, J. Native Iron Reduces CO2 to Intermediates and End-Products of the Acetyl-CoA Pathway. *Nat. Ecol. Evol.* **2018**, *2* (6), 1019–1024. https://doi.org/10.1038/s41559-018-0542-2.

(43) Preiner, M.; Igarashi, K.; Muchowska, K. B.; Yu, M.; Varma, S. J.; Kleinermanns, K.; Nobu, M. K.; Kamagata, Y.; Tüysüz, H.; Moran, J.; Martin, W. F. A Hydrogen-Dependent Geochemical Analogue of Primordial Carbon and Energy Metabolism. *Nat. Ecol. Evol.* **2020**, *4* (4), 534–542. https://doi.org/10.1038/s41559-020-1125-6.

(44) Yi, J.; Kaur, H.; Kazöne, W.; Rauscher, S. A.; Gravillier, L.-A.; Muchowska, K. B.; Moran, J. A Nonenzymatic Analog of Pyrimidine Nucleobase Biosynthesis. *Angew. Chem. Int. Ed.* **2022**, *61* (23), e202117211. https://doi.org/10.1002/anie.202117211.

(45) Rauscher, S. A.; Moran, J. Hydrogen Drives Part of the Reverse Krebs Cycle under Metal or Meteorite Catalysis. *Angew. Chem. Int. Ed.*, e202212932. https://doi.org/10.1002/anie.202212932.

(46) Smith, E.; Morowitz, H. J. Universality in Intermediary Metabolism. *Proc. Natl. Acad. Sci.* **2004**, *101* (36), 13168–13173. https://doi.org/10.1073/pnas.0404922101.

(47) Cleaves II, H. J. The Origin of the Biologically Coded Amino Acids. *J. Theor. Biol.* **2010**, *263* (4), 490–498. https://doi.org/10.1016/j.jtbi.2009.12.014.

(48) Austin, S. M.; Waddell, T. G. Prebiotic Synthesis of Vitamin B_6-Type Compounds. *Orig. Life Evol. Biosph.* **1999**, *29*, 287–296.

(49) Abundance of Elements in the Earth's Crust and in the Sea. In *CRC Handbook of Chemistry and Physics*; 2016; pp 14–17.

(50) Ueda, H.; Shibuya, T. Composition of the Primordial Ocean Just after Its Formation: Constraints from the Reactions between the Primitive Crust and a Strongly Acidic, CO_2-Rich Fluid at Elevated Temperatures and Pressures. *Minerals* **2021**, *11* (4), 389. https://doi.org/10.3390/min11040389.

(51) Jencks, W. P. *Catalysis in Chemistry and Enzymology*; McGraw-Hill: New-York, 1969.

(52) Robert, F.; Chaussidon, M. A Palaeotemperature Curve for the Precambrian Oceans Based on Silicon Isotopes in Cherts. *Nature* **2006**, *443* (7114), 969–972. https://doi.org/10.1038/nature05239.

(53) Krissansen-Totton, J.; Arney, G. N.; Catling, D. C. Constraining the Climate and Ocean PH of the Early Earth with a Geological Carbon Cycle Model. *Proc. Natl. Acad. Sci.* **2018**, *115* (16), 4105–4110. https://doi.org/10.1073/pnas.1721296115.

(54) Hızlı, S.; Karaoğlu, A. G.; Gören, A. Y.; Kobya, M. Identifying Geogenic and Anthropogenic Aluminum Pollution on Different Spatial Distributions and Removal of Natural Waters and Soil in Çanakkale, Turkey. *ACS Omega* **2023**, acsomega.2c07707. https://doi.org/10.1021/acsomega.2c07707.

(55) Mao, Z.; Campbell, C. T. Apparent Activation Energies in Complex Reaction Mechanisms: A Simple Relationship via Degrees of Rate Control. *ACS Catal.* **2019**, *9* (10), 9465–9473. https://doi.org/10.1021/acscatal.9b02761.

(56) Kozuch, S.; Martin, J. M. L. The Rate-Determining Step Is Dead. Long Live the Rate-Determining State! *ChemPhysChem* **2011**, *12* (8), 1413–1418. https://doi.org/10.1002/cphc.201100137.

(57) Abbott, E. H.; Martell, A. E. Nuclear Magnetic Resonance Spectra of Pyridoxylidene(Amino Acido)Aluminum(III) Complexes and Detection of a Possible General Intermediate in Metal-Catalyzed Reactions of Vitamin B_6. *J. Am. Chem. Soc.* **1973**, *95* (15), 5014–5019. https://doi.org/10.1021/ja00796a038.

(58) Murašková, V.; Szabó, N.; Pižl, M.; Hoskovcová, I.; Dušek, M.; Huber, Š.; Sedmidubský, D. Self Assembly of Dialkoxo Bridged Dinuclear Fe(III) Complex of Pyridoxal Schiff Base with CC Bond Formation – Structure, Spectral and Magnetic Properties. *Inorganica Chim. Acta* **2017**, *461*, 111–119. https://doi.org/10.1016/j.ica.2017.02.014.

(59) Blackmond, D. G. Reaction Progress Kinetic Analysis: A Powerful Methodology for Mechanistic Studies of Complex Catalytic Reactions. *Angew. Chem. Int. Ed.* **2005**, *44* (28), 4302–4320. https://doi.org/10.1002/anie.200462544.

(60) Burés, J. A Simple Graphical Method to Determine the Order in Catalyst. *Angew. Chem. Int. Ed.* **2016**, *55* (6), 2028–2031. https://doi.org/10.1002/anie.201508983.

(61) Nielsen, C. D.-T.; Burés, J. Visual Kinetic Analysis. *Chem. Sci.* **2019**, *10* (2), 348–353. https://doi.org/10.1039/C8SC04698K.

(62) Blake, M. I.; Siegel, F. P.; Katz, J. J.; Kilpatrick, M. Deuterium Isotope Effects in Transamination: L-Alanine and Pyridoxal. *J. Am. Chem. Soc.* **1963**, *85* (3), 294–297. https://doi.org/10.1021/ja00886a010.

(63) Julin, D. A.; Kirsch, J. F. Kinetic Isotope Effect Studies on Aspartate Aminotransferase: Evidence for a Concerted 1,3 Prototropic Shift Mechanism for the Cytoplasmic Isozyme and L-Aspartate and Dichotomy in Mechanism. *Biochemistry* **1989**, *28* (9), 3825–3833. https://doi.org/10.1021/bi00435a031.

(64) Kuramitsu, S.; Hiromi, K.; Hayashi, H.; Morino, Y.; Kagamiyama, H. Pre-Steady-State Kinetics of Escherichia Coli Aspartate Aminotransferase Catalyzed Reactions and Thermodynamic Aspects of Its Substrate Specificity. *Biochemistry* **1990**, *29* (23), 5469–5476. https://doi.org/10.1021/bi00475a010.

(65) Goldberg, J. M.; Kirsch, J. F. The Reaction Catalyzed by *Escherichia Coli* Aspartate Aminotransferase Has Multiple Partially Rate-Determining Steps, While That Catalyzed by the Y225F Mutant Is Dominated by Ketimine Hydrolysis. *Biochemistry* **1996**, *35* (16), 5280–5291. https://doi.org/10.1021/bi952138d.

(66) Albery, W. J.; Knowles, J. R. Evolution of Enzyme Function and the Development of Catalytic Efficiency. *Biochemistry* **1976**, *15* (25), 5631–5640. https://doi.org/10.1021/bi00670a032.

(67) Martell, A. E.; Taylor, P. NMR Evidence for the Delocalized .Alpha.,.Alpha.'-Carbanion of Pyridoxal and Pyridoxamine Schiff Bases as the Intermediate in Vitamin B6-Catalyzed Transamination. *Inorg. Chem.* **1984**, *23* (18), 2734–2735. https://doi.org/10.1021/ic00186a004.

(68) Rae, M.; Berberan-Santos, M. N. A Generalized Pre-Equilibrium Approximation in Chemical and Photophysical Kinetics. *J. Chem. Educ.* **2004**, *81* (3), 436. https://doi.org/10.1021/ed081p436.

(69) Kayser, R. H.; Pollack, R. M. Intramolecular General Base Catalysis of Schiff Base Hydrolysis by Carboxylate Ions. *J. Am. Chem. Soc.* **1977**, *99* (10), 3379–3387. https://doi.org/10.1021/ja00452a032.

(70) Kwan, E. E. Factors Affecting the Relative Efficiency of General Acid Catalysis. *J. Chem. Educ.* **2005**, *82* (7), 1026. https://doi.org/10.1021/ed082p1026.

(71) Toney, M. D.; Kirsch, J. F. Direct Brønsted Analysis of the Restoration of Activity to a Mutant Enzyme by Exogenous Amines. *Science* **1989**, *243* (4897), 1485–1488. https://doi.org/10.1126/science.2538921.

(72) Goldberg, J. M.; Kirsch, J. F. The Reaction Catalyzed by *Escherichia Coli* Aspartate Aminotransferase Has Multiple Partially Rate-Determining Steps, While That Catalyzed by the Y225F Mutant Is Dominated by Ketimine Hydrolysis. *Biochemistry* **1996**, *35* (16), 5280–5291. https://doi.org/10.1021/bi952138d.

(73) Cleland, W. W. What Limits the Rate of an Enzyme-Catalyzed Reaction. *Acc. Chem. Res.* **1975**, *8* (5), 145–151. https://doi.org/10.1021/ar50089a001.

(74) Dunathan, H. C. Stereochemical Aspects of Pyridoxal Phosphate Catalysis. In *Advances in Enzymology and Related Areas of Molecular Biology*; John Wiley & Sons, Ltd, 1971; pp 79–134. https://doi.org/10.1002/9780470122808.ch3.

(75) Kern, A. D.; Oliveira, M. A.; Coffino, P.; Hackert, M. L. Structure of Mammalian Ornithine Decarboxylase at 1.6 Å Resolution: Stereochemical Implications of PLP-Dependent Amino Acid Decarboxylases. *Structure* **1999**, *7* (5), 567–581. https://doi.org/10.1016/S0969-2126(99)80073-2.

For Table of Contents Only